

Reduced anharmonic phonon scattering cross-section slows the decrease of thermal conductivity with temperature

Xiaolong Yang ^{a, **}, Janak Tiwari ^b, Tianli Feng ^{b, *}

^a College of Physics and Center of Quantum Materials and Devices, Chongqing University, Chongqing, 401331, China

^b Department of Mechanical Engineering, University of Utah, Salt Lake City, UT, 84112, USA



ARTICLE INFO

Article history:

Received 26 January 2022

Received in revised form

30 March 2022

Accepted 1 April 2022

Available online 9 April 2022

Keywords:

Thermal conductivity

Lattice anharmonicity

Three-phonon scattering

Four-phonon scattering

Perturbation theory

Fermi's golden rule

ABSTRACT

Without anharmonic phonon scattering, crystals could have infinite or “super” intrinsic bulk thermal conductivity. Anharmonic phonon scattering rates usually increase with temperature, causing the decrease of thermal conductivity. In this work, we show that the increase of scattering rates is due to the increase of phonon population, while the anharmonic force constant, or phonon scattering cross-section, actually decreases with temperature in general solids. The decrease of scattering cross-section compensates the increase of population, slowing down the power-law increase of scattering rates and decrease of thermal conductivity. In other words, the use of temperature-dependent scattering cross-section increases the thermal conductivity relative to the 0 K ground-state scattering cross-section. We have demonstrated this effect by both first principles (for UO₂, Si, Ge, and w-BAs) and classical potentials (for general solids). As an example, after considering the temperature dependency of anharmonic force constants, we have predicted well the thermal conductivity for UO₂, which has long puzzled theoretical scientists, from room temperature up to 2000 K (available range of experimental data). The temperature-dependent scattering cross-section results in a more than 15 times increase of thermal conductivity at 2000 K compared to that predicted by using ground-state scattering cross-section. Four-phonon scattering becomes prominent at ultra-high temperature (>1500 K). This work is expected to inspire a broad study of thermal transport in various materials for both fundamental understanding and cutting-edge technologies.

© 2022 Elsevier Ltd. All rights reserved.

1. Introduction

Phonon is a quantization of nuclei vibration, carrying and transporting energy through interatomic interaction [1,2]. During the energy transport process, the creation and annihilation of phonons, as governed by Fermi's golden rule (FGR), determine the heat transport properties of most insulators and dielectrics. The net rates of phonon creation and annihilation, or the strength of phonon-phonon interaction, is proportional to both phonon populations and phonon-phonon scattering cross-section, or namely, phonon coupling constants [1–5]. The advancement of density functional theory (DFT) has enabled an accurate calculation of phonon-phonon coupling constants, and the combination with Boltzmann transport theory has enabled the first-principles

thermal conductivity (κ) prediction since 2007 [6]. As a result, the phonon κ of numerous materials has been predicted accurately and understood deeply since then [6–14]. Despite the great success, the predicted κ of many materials could still miss the experimental data significantly.

Uranium oxide (UO₂) is one example. As the most important nuclear fuel material, UO₂ has been extensively studied in the past 60 years and gained renewed interest by physicists in the recent decade [15–22]. Today UO₂ nuclear fuel contributes to nearly 20% of the world's electricity, and this number will likely increase significantly as the world is shifting towards 100% renewable energy. The further advancement of nuclear power efficiency needs a boost of the working temperature. The low thermal conductivity of UO₂ has been, however, the most serious limiting factor since it can lead to large centerline temperatures, pellet cracking, and fuel relocation [23]. Even worse, the thermal conductivity has not been understood or correctly predicted yet, i.e., the predicted thermal conductivity is more than 50% lower than experimental data even when only the lowest order of anharmonicity is included at high

** Corresponding author.

* Corresponding author.

E-mail addresses: yangxl@cqu.edu.cn (X. Yang), tianli.feng@utah.edu (T. Feng).

temperatures [15]. If higher-order anharmonicity is included, as needed when temperature increases and for anharmonic materials [8–10,12,13,24], the prediction would become even lower. Not only for UO_2 , but many other materials, the predicted thermal conductivity by the state-of-the-art first-principles methods with three and four-phonon scattering being included is much lower than experimental data [9].

In this work, using UO_2 as an example, with several different methods of predicting κ , we find that the temperature impact on anharmonic interatomic force constants (IFCs) plays the most significant role in accurately predicting the thermal conductivity at high temperatures. As temperature increases, the phonon population increases, which increases the phonon scattering rates. However, the temperature rise can also reduce the scattering probability (or scattering cross-section), which reduces the phonon scattering rates. These two factors compete with each other, leading to a much flatter κ as a function of T than the power law T^{-1} or T^{-2} . Our predicted thermal conductivity of UO_2 reproduces well the measured data throughout a wide temperature range up to 2000 K (available range for experimental measurement). To examine whether the phenomenon that anharmonic phonon scattering cross-section decreases with temperature is a special characteristic only for UO_2 or true for other materials as well, we test silicon (Si), germanium (Ge), and wurtzite boron arsenide (w-BAs), three strongly harmonic materials, and find the same conclusion. This effect is very small for strongly harmonic systems, being part of the reason why it was not found previously. For further examination, we test classical interatomic potentials since they have been well established to describe thermal transport in various materials for many years, and the same conclusion is found: phonon scattering cross-section decreases with temperature.

2. Methods

In the standard Peierls Boltzmann transport equation (BTE), the thermal conductivity along the direction x is calculated by Refs. [25,26],

$$\kappa_p^{xx} = \frac{1}{V} \sum_{\lambda} v_{x,\lambda}^2 c_{\lambda} \tau_{\lambda}^{it} \quad (1)$$

Here the subscript ‘‘P’’ of κ_p^{xx} stands for standard phonon Peierls (population) thermal conductivity, to distinguish from the interband (coherence) thermal conductivity κ_c^{xx} induced by the interband crossover coherence [9,10,24,27,28]. Without explicit clarification, the standard Peierls κ_p^{xx} is written as κ in the subsequent text. Here λ is short for a phonon mode (\mathbf{q}, j) with \mathbf{q} and j labeling the phonon wave vector and dispersion branch, respectively. V is crystal volume, v_{α} is phonon group velocity projection along α , and c_{λ} is phonon specific heat per mode. τ_{λ}^{it} is the phonon lifetime solved by an iterative scheme, which could include three-phonon (3ph), four-phonon (4ph), and isotope scattering rates: $\tau_{3,\lambda}^{-1}$, $\tau_{4,\lambda}^{-1}$, and $\tau_{iso,\lambda}^{-1}$. The evaluation of τ or scattering rate τ^{-1} requires anharmonic IFCs using Fermi’s golden rule.

Tracing back the history of first-principles prediction of κ using BTE, the method development has experienced three great advancements, as illustrated in Fig. 1 (a) as I, II, and III, respectively. The first one was done by Broido et al. [6], who, for the first time, integrated all phonon modes’ lifetimes τ_{λ} in the whole Brillouin zone with BTE to calculate κ . This method achieved great success as it has boosted the predictions of numerous new materials [7,14]. In this method, the phonon lifetimes τ_{λ} are calculated through 3ph scattering using the 3rd-order IFCs obtained at the ground state (0 K). The second advancement was made by Feng and Ruan [12],

who realized rigorous 4ph scattering calculation and integrated it with BTE. Four-phonon scattering has been recognized to considerably reduce κ of a broad range of materials [8–10,12,13,24]. In this method, the 4th-order IFCs are required. The third advancement was made by Xia [29] as well as Ravichandran and Broido [30], who replaced the ground state phonon dispersion with a temperature-dependent (TD) one and found a great increase of predicted κ , which compensates the decrease by 4ph scattering in some materials [9,10,24,29,30]. We employed all Methods I, II, and III for calculating the thermal conductivity UO_2 (lattice structure shown in Fig. 1 (b)) from 0 to 2000 K. The details of thermal conductivity formalisms, 3ph and 4ph scattering formalisms, phonon-defect scattering formalism, 2nd, 3rd, and 4th order IFCs calculations can be found in the Supplemental Material.

3. Results

We find that none of Methods I, II, and III can provide a good prediction for UO_2 . Specifically, the prediction is around 1.5 W/m-K at 1200 K, which mispredicted the experimental data 3.5 W/m-K by 57%. If four-phonon scattering is included, as needed for anharmonic materials [8–10,12,13,24], the prediction would become even worse as it would further decrease the predicted κ . As shown in Fig. 1 (c). The predicted thermal conductivities using Methods I, II, III, and their combinations, 0.75–2 W/m-K at 1200 K, are much lower than experimental 3.5 W/m-K.

Inspired by the fact that the lattice has a large softening effect at high temperatures while none of the Methods I, II, and III has taken into account temperature-dependent anharmonic IFCs (or phonon scattering cross-section), we proposed a Method IV, as shown in Fig. 1 (a), to employ the temperature effect on all harmonic and anharmonic IFCs. Since the calculation of temperature-dependent anharmonic 3rd and 4th-order IFCs from ab initio molecular dynamics (AIMD) is computationally demanding, here we employ a machine learning method to reproduce the AIMD energy surface, and the details are given in the Supplemental Material. The high accuracy of this method has been demonstrated in a recent work [35]. Intuitively, anharmonicity increases with temperature [2,36,37], and the employment of temperature-dependent IFCs will further decrease the predicted κ as atoms deviate more from their harmonic potential well (e.g., equilibrium position) at higher temperatures. However, on the contrary, the predicted κ is increased and matches reasonably well with experimental data throughout the temperature range up to 2000 K, as shown in Fig. 1 (d). As seen in Fig. 1 (e), the predicted κ using temperature-dependent anharmonic IFCs is ~15 times larger than the one predicted by using ground state 0 K anharmonic IFCs at 2000 K.

The κ increase after considering temperature-dependent anharmonic IFCs is totally different from the κ increase after considering temperature-dependent phonon dispersion observed in Refs. [9,10,24,29,30]. In those works, the temperature effect tunes phonon dispersion, allowing fewer scattering processes restricted by energy and momentum selection rules, which increases thermal conductivity. In contrast, in the present work, the number of allowed scattering processes does not change much, but the scattering probability of each process reduces significantly due to the decrease of phonon scattering cross-section. That is, the temperature effect reduces phonon scattering cross-section and scattering probability. In fact, if we only consider the temperature effect on phonon dispersion or the effect on energy and momentum selection rules, the thermal conductivity would even decrease (see the triangles as compared to circles in Fig. 1 (c)). This effect can be seen clearly in Fig. 2. The phonon dispersion softening effect reduces thermal conductivity, while the anharmonic scattering softening effect increases the thermal conductivity.

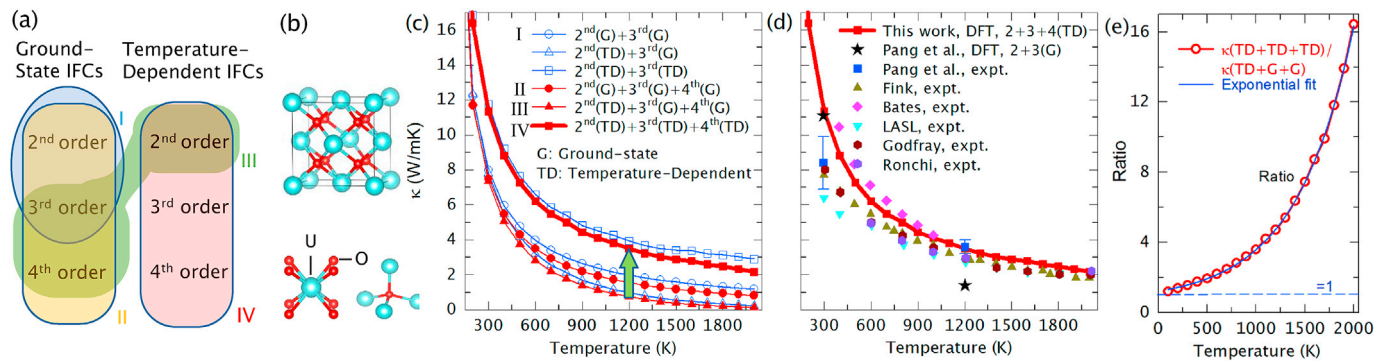


Fig. 1. Thermal conductivity of UO_2 calculated from first principles-based BTE methods. (a) Methods of predicting κ based on BTE. The literature works have employed Method I, II, and III. This work exploits Method IV. (b) Lattice structure of UO_2 . (c) Predicted κ of UO_2 using various methods. (d) The predicted κ compared to available experimental data [15,16,31–34]. The first-principles results (black star) from Pang et al. [15] using ground-state 3rd order IFCs are also included for comparison. (e) The ratio of $\kappa(\text{TD})$ to $\kappa(\text{G})$ as a function of T . The green arrow in (c) demonstrates the increase of κ after including finite-temperature anharmonic IFCs.

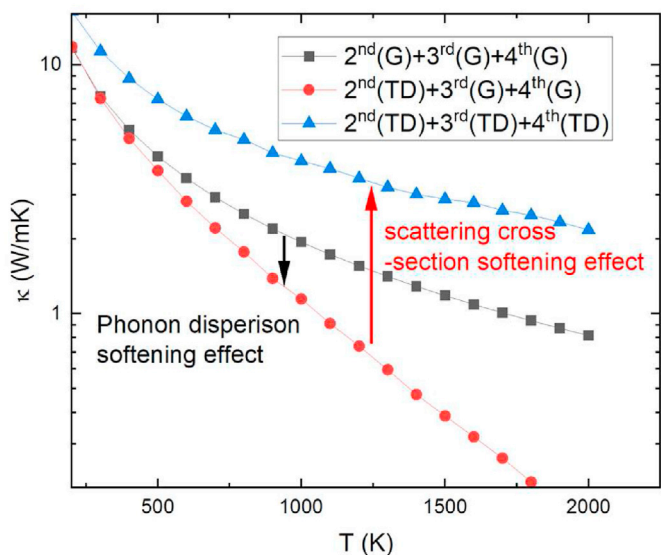


Fig. 2. Thermal conductivity of UO_2 affected by phonon dispersion and scattering cross-section softening effects.

Further evidence could be found in Fig. 3: the phonon group velocity after using temperature-dependent IFCs reduces slightly, impossible to contribute to κ increase; it is the Grüneisen

parameter (anharmonicity) and phonon scattering rates reduction that increases κ . Also, such reduction is more for 1200 K than for 300 K (Fig. 3 (c) and (d)), supporting that phonon scattering cross-section is smaller at higher temperatures. Furthermore, the 4ph scattering rates are decreased more than the 3ph scattering rates relatively, indicating that the quartic anharmonicity is weakened more than the cubic anharmonicity at finite temperatures.

Fig. 4 shows the comparison between phonon scattering rates before and after considering the temperature dependence of anharmonic IFCs. In all cases, the temperature dependence of 2nd-order harmonic IFCs are considered. Clearly, before considering the temperature-dependent anharmonic IFCs, phonon scattering rates increase with temperature as T^α . After considering the temperature effect on anharmonic IFCs, phonon scattering rates increase slowly with temperature and exhibit a saturation trend. The ratio $\tau^{-1}(\text{TD})/\tau^{-1}(\text{G})$ decrease with temperature significantly, which is due to the softening of anharmonic IFCs, or the softening of scattering cross-section.

For many applications, the phonon mean free path (MFP) spectra can provide crucial information about the impact of grain size on thermal conductivity. As shown in Fig. 5 (b), the dominant phonon MFP in UO_2 at 300 K is below 100 nm (corresponding to phonons with energy below 40 meV, see Fig. 5 (a)), and this value decreases to 20 nm and 5 nm at 1200 and 2000 K, respectively. This information indicates that in most nuclear fuels, the phonon thermal conductivity is probably not affected by grain boundaries while other defects and bubbles might play a more important role [38–48]. The spectral κ and its accumulation with frequency are

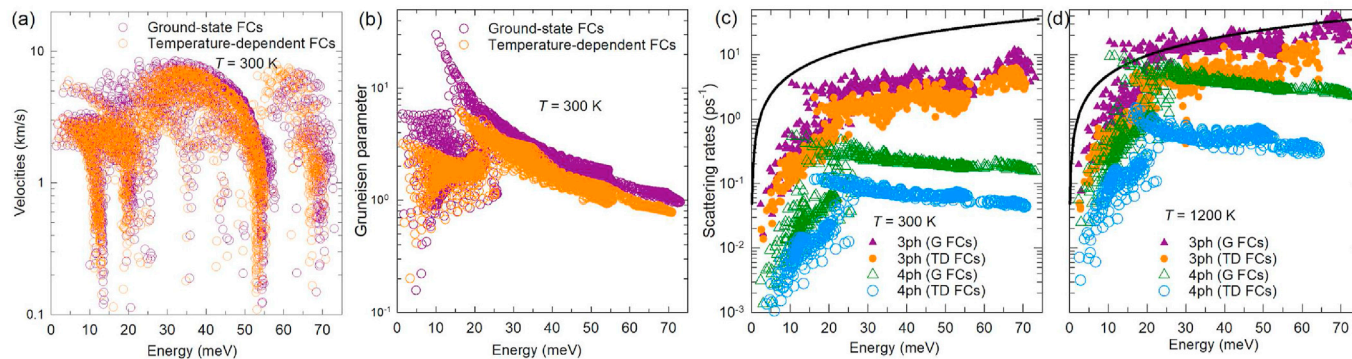


Fig. 3. Comparison between phonon properties of UO_2 calculated using ground-state and temperature-dependent IFCs. (a) Phonon group velocities at 300 K. (b) Phonon Grüneisen parameter at 300 K. (c) Three and four-phonon scattering rates at 300 K. (d) Three and four-phonon scattering rates at 1200 K. The black lines are twice the phonon frequency [24] to guide the eyes.

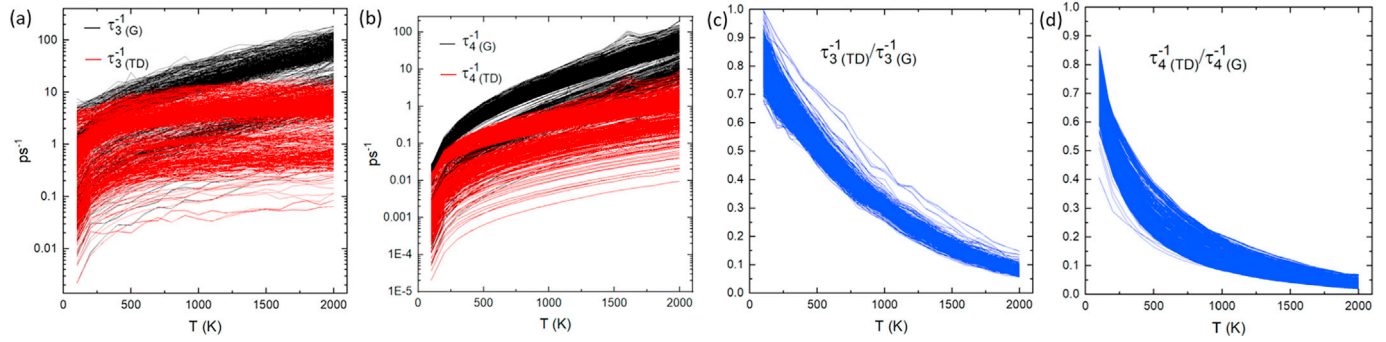


Fig. 4. The direct comparison between scattering rates before and after including temperature effect on scattering cross-section in UO_2 . The 2nd-order harmonic IFCs are the same in all cases. Different curves represent different phonon modes throughout the Brillouin zone and all phonon branches.

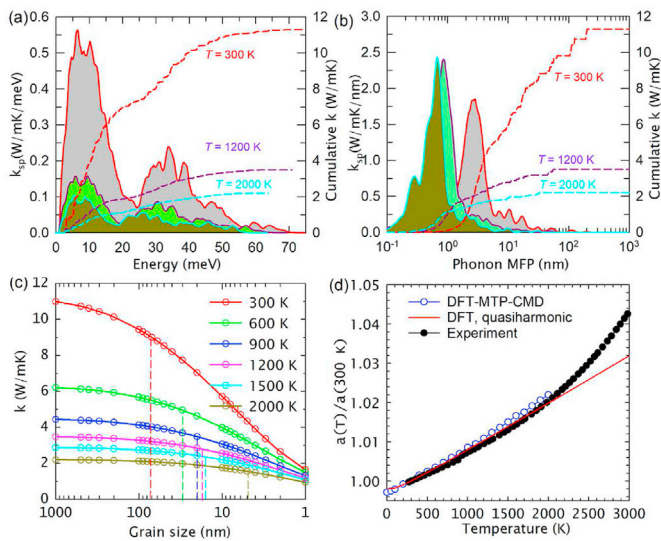


Fig. 5. (a) Spectral and cumulative κ of UO_2 as a function of phonon energy at 300, 1200, and 2000 K. (b) Spectral and cumulative κ as a function of phonon MFP. (c) Phonon κ as a function of grain size. The dashed lines indicate the grain sizes at which phonon κ is reduced by 20% compared to the bulk value. (d) Relative lattice constant change as a function of temperature: comparison between DFT calculations in this work and the fitting of a large set of experimental data from Ref. [31].

shown in Fig. 5 (a). Optical branches are found to contribute 40–50% to the total thermal conductivity throughout the temperature range, agreeing well with experimental conclusions [15]. The thermal expansion coefficient is also crucial for nuclear cells. Our work predicted well the lattice expansion throughout the temperature range by using equilibrium molecular dynamics simulations. The quasiharmonic approximation prediction also matches well with the experiment below 2000 K, but underestimates the lattice expansion above that temperature. The bulk modulus calculated in this work is 2083.5 kbar, close to the experimental data 2127 kbar [49]. The method of quasiharmonic lattice expansion coefficient calculation is the same as Ref. [50]. The impacts of oxygen vacancy and uranium vacancy defects, which are crucial for thermal engineering of UO_2 , are found to be significant and are discussed in the Supplemental Material.

In this work, we do not compare our UO_2 thermal conductivity prediction with those predicted by empirical potentials-based classical molecular dynamics in the literature [16,22,38–41, 44–46,51–57]. As studied by Ref. [58], empirical potentials can only reasonably predict well the acoustic phonon dispersion, but severely mispredict the optical phonon dispersion. Some empirical

potentials significantly underestimate κ and some overestimate κ . For those that could agree with the experiment, it is more like a coincidence since they largely overestimate the acoustic phonon thermal contribution while underestimating the optical phonon thermal contribution, making the total match with the experiment. Also, we intentionally do not compare the scattering rate with the INS linewidth because the latter is subject to a smearing/broadening effect due to the finite resolution of \mathbf{q} point in the INS measurement.

We want to note some limitations of the methods used in the paper. (1) To extract the IFCs, the TDEP methods based on molecular dynamics is used. Since molecular dynamics intrinsically uses classical temperature, its classical Boltzmann statistics has an intrinsic discrepancy to describe the Bose-Einstein statistics. Therefore, this method is applicable only at high temperatures when thermal energy ($k_B T$) is much higher than phonon energy ($\hbar\omega$). Considering the Debye temperature of UO_2 is around 377 K [59], which is at the bottom of the temperature range we study, we expect most of the results in this paper are not affected significantly. (2) The four-phonon scattering in this paper is still within the relaxation time approximation framework, which might underpredict the thermal conductivity compared to the full solution. We expect that this underprediction is negligible for UO_2 as the Umklapp process dominates four-phonon scattering. (3) The radiation contribution to thermal conductivity at high temperatures is neglected. We considered the possibility of radiation by using the Rosseland model. However, due to the lack of reliable experimental data of absorption coefficients and dielectric function, no conclusion could be drawn at this point. (4) The exchange-correlation function used in DFT simulations can also have impact on the final results [60]. Here, we focus on self-consistent comparisons.

4. Discussions

4.1. Phonon scattering cross-section

To gain more physical insights into the decrease of phonon scattering rates and the increase of thermal conductivity after including the temperature impact on anharmonic IFCs, we start by examining the formalism of lattice anharmonicity as well as phonon scattering rates. The Hamiltonian of a crystal is [3,12,61].

$$\hat{H} = \hat{H}_0 + \sum_{\lambda_1 \lambda_2 \lambda_3} H_{\lambda_1 \lambda_2 \lambda_3}^{(3)} A_{\lambda_1 \lambda_2 \lambda_3} + \sum_{\lambda_1 \lambda_2 \lambda_3 \lambda_4} H_{\lambda_1 \lambda_2 \lambda_3 \lambda_4}^{(4)} A_{\lambda_1 \lambda_2 \lambda_3 \lambda_4} + \dots \quad (2)$$

where \hat{H}_0 is the harmonic term and the other two are third-order

and fourth-order anharmonic terms. $H_{\lambda_1\lambda_2\lambda_3}^{(3)}$ and $H_{\lambda_1\lambda_2\lambda_3\lambda_4}^{(4)}$ are the 3ph and 4ph coupling constants, which are determined by anharmonic force constants. $A_{\lambda_1\lambda_2\lambda_3}$ and $A_{\lambda_1\lambda_2\lambda_3\lambda_4}$ are phonon operators that determine phonon populations [3,12,61]. λ_i denotes phonon modes. Based on Eq. (2), it is found that the lattice anharmonicity is determined by two properties: the anharmonic phonon coupling constant (e.g., $H_{\lambda_1\lambda_2\lambda_3}^{(3)}$ and $H_{\lambda_1\lambda_2\lambda_3\lambda_4}^{(4)}$) and the phonon population (e.g., $A_{\lambda_1\lambda_2\lambda_3}$ and $A_{\lambda_1\lambda_2\lambda_3\lambda_4}$). The former is determined by anharmonic IFCs, and the latter is determined by temperature (or displacement amplitude of atoms from their equilibrium positions).

With FGR, the phonon-phonon scattering rates are

$$\tau_{\lambda}^{-1} = \sum_{\lambda_1\lambda_2} N_{\lambda_1\lambda_2} \mathcal{S}^{(3)} + \sum_{\lambda_1\lambda_2\lambda_3} N_{\lambda_1\lambda_2\lambda_3} \mathcal{S}^{(4)} + \dots, \quad (3)$$

where $\mathcal{S}^{(3)}$ and $\mathcal{S}^{(4)}$, describing the scattering probability, can be regarded as phonon scattering cross-section based on the terminology “cross-section” used in particle physics in describing the ratio of scattered power in total incident power. $\mathcal{S}^{(3)}$ and $\mathcal{S}^{(4)}$ are originated from $H_{\lambda_1\lambda_2\lambda_3}^{(3)}$ and $H_{\lambda_1\lambda_2\lambda_3\lambda_4}^{(4)}$, respectively. $N_{\lambda_1\lambda_2}$ and $N_{\lambda_1\lambda_2\lambda_3}$, two quantities that depend on Bose-Einstein phonon population $n_{\lambda_1}^0$, $n_{\lambda_2}^0$, and $n_{\lambda_3}^0$, are originated from $A_{\lambda_1\lambda_2\lambda_3}$ and $A_{\lambda_1\lambda_2\lambda_3\lambda_4}$, respectively. $N_{\lambda_1\lambda_2}$ and $N_{\lambda_1\lambda_2\lambda_3}$ are proportional to phonon population and its square, respectively. For example, for splitting processes, $N_{\lambda_1\lambda_2} = \frac{1}{2}(1 + n_{\lambda_1}^0 + n_{\lambda_2}^0)$, $N_{\lambda_1\lambda_2\lambda_3} = \frac{1}{6}n_{\lambda_1}^0 n_{\lambda_2}^0 n_{\lambda_3}^0 / n_{\lambda}^0$ (see Supplemental Material Section A for details). Based on Eq. (3), it is found that the phonon scattering rate is determined by two properties: the phonon scattering probability or cross-section (e.g., $\mathcal{S}^{(3)}$ and $\mathcal{S}^{(4)}$) and the phonon population (e.g., $N_{\lambda_1\lambda_2}$ and $N_{\lambda_1\lambda_2\lambda_3}$). The former is determined by anharmonic IFCs, and the latter is determined by temperature (or kinetic energy of atoms).

As temperature increases, $N_{\lambda_1\lambda_2}$ and $N_{\lambda_1\lambda_2\lambda_3}$ increases linearly and quadratically, which tend to increase phonon-phonon scattering rates (τ_{λ}^{-1}) linearly and quadratically with temperature, respectively. Meanwhile, the scattering cross-section $\mathcal{S}^{(3)}$ and $\mathcal{S}^{(4)}$ decrease with temperature, which tends to decrease the phonon-phonon scattering rates. With this competition, the phonon scattering rate may or may not increase with temperature. This competition is demonstrated in Fig. 6: temperature increases phonon population but decreases phonon scattering probability. Previously, the temperature impact on phonon scattering

probability ($\mathcal{S}^{(3)}$ and $\mathcal{S}^{(4)}$) is ignored, leading to a conclusion that τ_{λ}^{-1} scales as $\sim T^{\alpha}$ with temperature, where $\alpha = 1$ for 3ph and 2 for 4ph processes [8,12,62]. Now, with temperature impact on anharmonic IFCs, this scaling law changes to $\sim T^{\alpha}f(T)$, where $f(T)$ is a decreasing function with temperature determined by the temperature dependency of scattering cross-section or anharmonic IFCs.

For UO_2 , we fitted $f(T)$ as $\exp(-AT)$, where A is some immaterial constant. This can be estimated by the following way. The ratio of $\kappa(\text{TD})$ and $\kappa(\text{G})$ is plotted in Fig. 1 e, where $\kappa(\text{TD})$ and $\kappa(\text{G})$ are predicted by using temperature-dependent and ground-state anharmonic IFCs, respectively. We find that $\frac{\kappa(\text{TD})}{\kappa(\text{G})}$ is fitted very well by $\sim \exp(AT)$. That is, roughly, $\frac{\tau_{\lambda}^{-1}(\text{TD})}{\tau_{\lambda}^{-1}(\text{G})} \sim \frac{\kappa(\text{G})}{\kappa(\text{TD})} \sim \exp(-AT)$. Therefore, the anharmonic IFCs should also decrease exponentially with temperature: $\left| \frac{\varphi_{\text{TD}}^{(n)}}{\varphi_{\text{G}}^{(n)}} \right| \sim \frac{\sqrt{\tau_{\lambda}^{-1}(\text{TD})}}{\sqrt{\tau_{\lambda}^{-1}(\text{G})}} \sim \exp(-\frac{AT}{2})$. Note that the fact “phonon scattering cross-section decreases with temperature” does not mean “thermal conductivity increases with temperature”. Actually, $\kappa(\text{TD}) \sim \kappa(\text{G})e^{AT} \sim T^{-\alpha}e^{AT}$. Note that the exponential form of $f(T)$ is numerical fitting results for UO_2 only. For other materials, the form of $f(T)$ could be complicated as seen in Si and Ge in the following discussion.

It is worth noting that the previous conclusion that “4ph scattering becomes more important at a higher temperature” [8–10,12,13,24] does not conflict with our conclusion that “phonon scattering cross-section decreases with temperature”. The 4ph scattering becomes more important at a higher temperature because more phonon population is excited at a higher temperature, allowing more 4ph scattering than 3ph scattering since 4ph scattering rates scale quadratically with phonon population while 3ph scattering rates scales linearly. That is, $\tau_{4\text{ph}}^{-1} \sim T^2$ increases faster than $\tau_{3\text{ph}}^{-1} \sim T$ with temperature at higher temperatures. The phonon scattering cross-section actually decreases with temperature for both.

Note that even after including 4ph scattering, the phonon linewidth does not exceed twice the phonon frequency [24], indicating that most phonons are still reasonably well defined even at high temperatures (See Fig. 3 and Supplemental Figures). If the phonon scattering cross-section reduction effect is not included, phonon linewidths could become too large that the phonon gas model is not valid anymore [63].

To further examine whether the phonon scattering cross-section reduction effect is unique for UO_2 or broadly applicable to

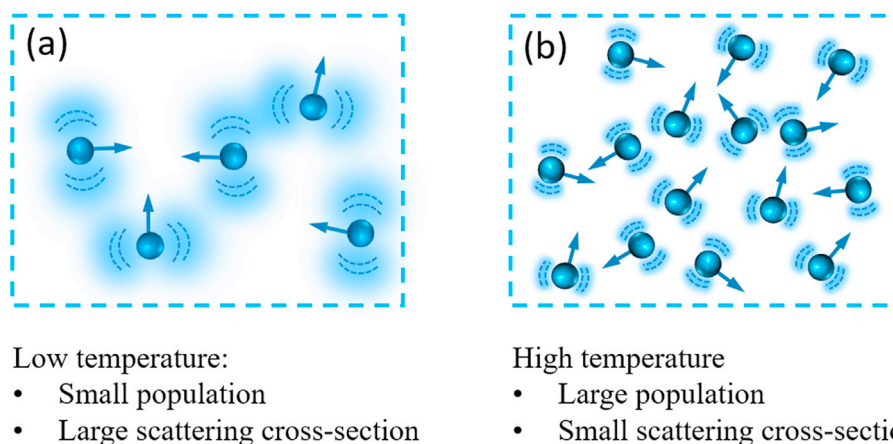


Fig. 6. Sketch to demonstrate the temperature impacts on phonon scattering: increasing temperature increases phonon population but decreases the scattering cross-section between phonons. Each sphere in the figure represents a phonon. The sizes of dashed circles indicate the relative amplitudes of scattering cross-section.

other materials, we examine the temperature-dependent anharmonic force constants for silicon and germanium, two commonly used materials for basic theory benchmarking. As shown in Fig. 7, the anharmonic force constants reduction effect is a much more common characteristic than thought. For both Si and Ge, although there are some IFCs that increase with temperature, most of them decrease. We note that the IFCs do not necessarily decrease exponentially - they can also decrease linearly or polynomially. At this point, we do not have a clear mathematical form for the IFCs as a function of temperature. It could be complicated and material dependent. It is determined by how the average interatomic forces change with increased atoms' displacements. The centers of displacements, i.e., equilibrium positions, also change with temperature.

For Si and Ge, we have also calculated their thermal conductivity in a testing manner, since a large q-mesh ($16 \times 16 \times 16$) is necessary to get a converged thermal conductivity for Si and Ge, which is beyond our simulation capability. We calculated their thermal conductivities using a $12 \times 12 \times 12$ q-mesh as shown in Fig. S3 in the Supplemental Material. We find that, the thermal conductivity after considering temperature-dependent anharmonic IFCs is higher than that using ground-state anharmonic IFCs, further supporting our previous conclusion. The ratio $\kappa_{34(TD)}/\kappa_{34(G)}$ increases with temperature, but the increase is much smaller than that in UO_2 . This is understandable because a number of IFCs in Si and Ge exhibit almost linear or very weak temperature dependence, probably due to weak anharmonic effects in these two materials. Despite the fact that scattering cross-section would decrease with increasing temperature, it would hardly have notable impact on thermal conductivity. We also note that the effect in Ge is larger than that in Si. This indicates that the softening effect is stronger for materials with stronger anharmonicity.

We note that a recent work has calculated the thermal conductivity of *w*-BAs [35]. We observed similar phenomenon, i.e., the temperature-dependent anharmonic IFCs give larger thermal conductivity than that given by 0 K IFCs. The effect in *w*-BAs is small compared to UO_2 . Based on these observations, we conclude that the temperature softening effect in the anharmonic IFCs is plausibly stronger for more strongly anharmonic materials, and it increases with temperature.

To gain more direct insight, we examine classical potentials because classical potential is an effective, simple, clear, and commonly used method to describe the interatomic interactions and has been well benchmarked in various materials for thermal properties. We select some representative classical potentials, including Lennard-Jones, Lennard-Jones 96, Morse, and

Buckingham, to calculate the 2nd, 3rd, and 4th order IFCs as a function of interatomic distance r , as shown in Fig. 8. Inspiringly, they all show decreasing harmonic and anharmonic IFCs with r_0 . Since r_0 is a positive function of T (due to the positive thermal expansion), we can conclude that IFCs also decrease with T . The positive thermal expansion can be seen from the increased average r as the vibration amplitude increases in Fig. 8. Note that Fig. 8 shows r -dependent IFCs rather than T -dependent IFCs. To calculate T -dependent IFCs, as done for UO_2 , Si, and Ge in this work, one should consider the vibrational amplitude of atoms at a certain temperature like in the TDEP method. Nonetheless, Fig. 8 is enough to support our hypothesis, i.e., in addition to bond softening, anharmonic force constants are also softened with temperature in general solids. Here we do not exclude the possibility of the existence of exceptions, e.g., negative-thermal expansion materials.

4.2. Off-diagonal coherence phonon thermal conductivity

For materials with low thermal conductivity, it is necessary to check if the interband thermal conductivity is large or not [9,10,24,27,28]. In the Wigner formalism, the lattice thermal conductivity component $\kappa_L^{\alpha\beta}$ is

$$\kappa_L^{\alpha\beta} = \kappa_P^{\alpha\beta} + \kappa_C^{\alpha\beta} = \frac{\hbar^2}{k_B T^2 V N_{\mathbf{q}}} \sum_{\mathbf{q}} \sum_{j,j'}^{3n_b, 3n_b} v_{\mathbf{q},jj'}^{\alpha} v_{\mathbf{q},jj'}^{\beta} \frac{\omega_{\mathbf{q},j} + \omega_{\mathbf{q},j'}}{2} \frac{\omega_{\mathbf{q},j} n_{\mathbf{q},j} (n_{\mathbf{q},j} + 1) + \omega_{\mathbf{q},j'} n_{\mathbf{q},j'} (n_{\mathbf{q},j'} + 1)}{4(\omega_{\mathbf{q},j'} - \omega_{\mathbf{q},j})^2 + (\tau_{\mathbf{q},j}^{-1} + \tau_{\mathbf{q},j'}^{-1})^2} (\tau_{\mathbf{q},j}^{-1} + \tau_{\mathbf{q},j'}^{-1}) \quad (4)$$

Here α and β represent the Cartesian directions x, y and z . The subscript "L" represent lattice. The standard Peierls thermal conductivity $\kappa_P^{\alpha\beta}$ can be obtained by enforcing the phonon branch $j = j'$ in the summation, while the interband $\kappa_C^{\alpha\beta}$ is obtained by making $j \neq j'$ in the summation. In the equation above, V is the volume of a primitive cell, $N_{\mathbf{q}}$ is total number of sampled \mathbf{q} points, n_b is the number of atoms in primitive cell, and $n_{\mathbf{q},j}$ is the Bose-Einstein phonon population of mode (\mathbf{q}, j) . The interband velocity matrix element $v_{\mathbf{q},jj'}^{\alpha}$ is obtained by

$$v_{\mathbf{q},jj'}^{\alpha} = \sum_{b_1, \alpha_1, b_2, \alpha_2}^{n_b, 3, n_b, 3} \varepsilon_{\mathbf{q},j, b_1, \alpha_1}^* \frac{\partial}{\partial \mathbf{q}_{\alpha}} \left[\left(\sqrt{\mathbf{D}(\mathbf{q})} \right)_{b_1, \alpha_1, b_2, \alpha_2} \right] \varepsilon_{\mathbf{q},j', b_2, \alpha_2} \quad (5)$$

Here, b_1 and b_2 are indices of basis atoms in the primitive cell, ε and ε^* are the eigenvector component and its conjugate, and \mathbf{D} is

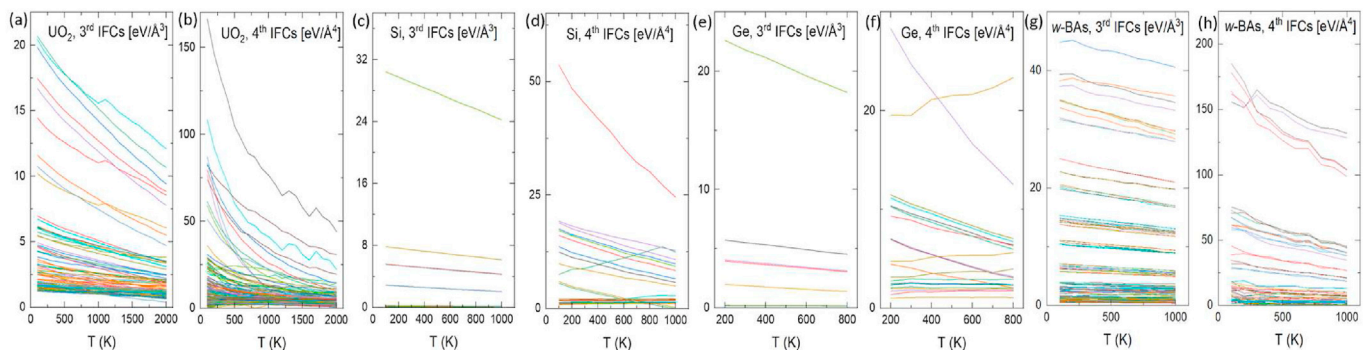


Fig. 7. Temperature-dependent IFCs of UO_2 , Si, Ge, and *w*-BAs. (a,c,e,g) 3rd-order IFCs. (b,d,f,h) 4th-order IFCs. In each sub-figure, different curves represent different force constant elements in the IFC matrix. Numerous trivial force constant elements with values close to zero are not shown, to mitigate the complexity in plotting. Note that the IFCs are obtained from molecular dynamics simulations that have considered the larger vibrational amplitude of atoms at higher temperatures, rather than from perturbation theory that calculates IFCs only at the equilibrium position in an expanded lattice. The scattering cross-section is proportional to the square of the IFCs.

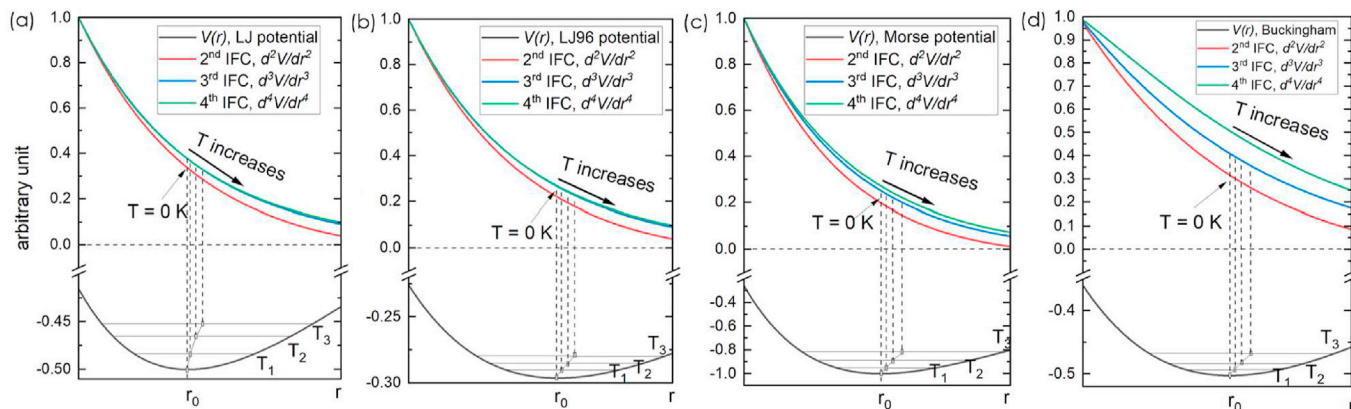


Fig. 8. Classical interatomic potential $V(r)$ and its 2nd, 3rd, and 4th-order derivatives with respect to r . (a)–(d) are the Lennard-Jones potential $V_{LJ} \sim (\frac{r}{\sigma})^{12} - (\frac{r}{\sigma})^6$, Lennard-Jones 96 potential $V_{LJ96} \sim (\frac{r}{\sigma})^9 - (\frac{r}{\sigma})^6$, Morse potential $V_{Morse} \sim (1 - e^{-a(r-r_0)^2}) - 1$, and Buckingham potential $V_{Buck} \sim Aexp(-Br) - C/r^6$, respectively.

the dynamical matrix. Note that the square root is applied on the whole \mathbf{D} matrix rather than on the \mathbf{D} elements.

The calculated interband thermal conductivity is shown in Fig. 9, as compared to the standard Peierls thermal conductivity. The interband κ_C is relatively small, which is because UO_2 has a small primitive cell and the overlapping between different phonon bands is not as significant as complex crystals [9,10,24,27,28]. As temperature increases, the interband κ_C becomes non-negligible.

5. Conclusions

To summarize, we find that the phonon scattering cross-section, or scattering probability, decreases with temperature, although the total phonon scattering rates and thermal resistance may still increase with temperature. This finding could solve a long puzzle why the thermal conductivity of many materials does not follow the power law $\sim T^\alpha$ at high temperatures. As temperature increases, phonon population increases, which tends to increase the phonon scattering rates by $\sim T^\alpha$ and decreases the thermal conductivity by $\sim T^{-\alpha}$. However, as temperature increases, phonon scattering cross-section decreases, at a speed of $\exp(-AT)$ or linearly, tending to slow the decrease of scattering rates and increase of thermal

conductivity. For UO_2 , this effect results in more than 15 times increase of thermal conductivity at 2000 K. With a general examination, we conclude that this is not a special case for specific materials but should be common characteristic for general solid. Exceptions may exist though, which requires future efforts. We expect our findings provide new insight into phonon transport and will inspire the study in numerous materials and applications.

Data availability

Source data are provided with this paper. All other data that support the plots within this paper are available from the corresponding authors on reasonable request.

Code availability

The codes used in this study are available from the corresponding authors upon request.

Credit author statement

Tianli Feng: Conceptualization, Supervision, Writing- Original draft preparation. **Xiaolong Yang:** Simulation, Data Analysis, Writing- Reviewing and Editing. **Janak Tiwari:** Simulation, Writing- Reviewing and Editing.

Declaration of competing interest

The authors declare that they have no known competing financial interests or personal relationships that could have appeared to influence the work reported in this paper.

Acknowledgments

X.Y. acknowledges the support from the Natural Science Foundation of China (Grant No. 12004254) and the startup funding from Chongqing University (Grant No. 0233001104472). J.T. and T.F. acknowledge the startup funding support from the University of Utah. The support and resources from the Center for High Performance Computing at the University of Utah are gratefully acknowledged.

Appendix A. Supplementary data

Supplementary data to this article can be found online at <https://doi.org/10.1016/j.mtphys.2022.100689>.

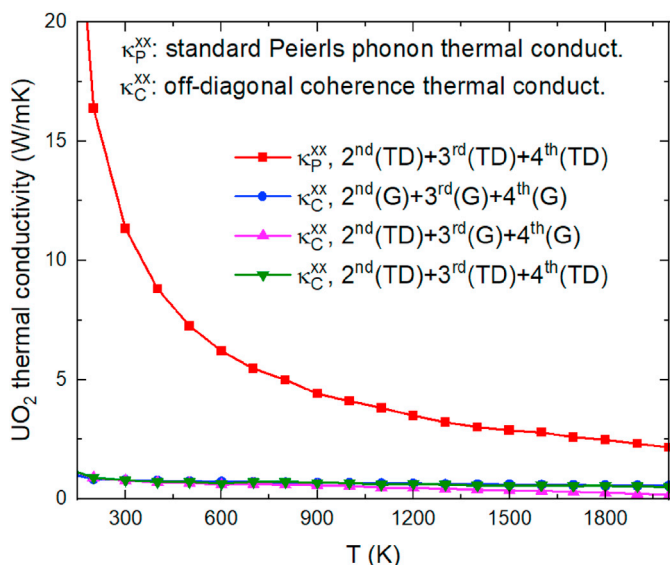


Fig. 9. First-principles calculated interband coherence thermal conductivity (κ_C^{xx}) compared to the standard Peierls thermal conductivity (κ_P^{xx}) for UO_2 .

References

- [1] J.M. Ziman, *Electrons and Phonons: the Theory of Transport Phenomena in Solids*, Oxford university press, 1960.
- [2] M. Dove, *Introduction to Lattice Dynamics*, Cambridge University Press, New York, New York, USA, 1993.
- [3] A. Maradudin, A. Fein, Scattering of neutrons by an anharmonic crystal, *Phys. Rev.* 128 (1962) 2589.
- [4] A.A. Maradudin, P.A. Flinn, Anharmonic contributions to vibrational thermodynamic properties of solids: Part I, *Ann. Phys.* 15 (1961) 337.
- [5] A.A. Maradudin, A.E. Fein, G.H. Vineyard, On the evaluation of phonon widths and shifts, *Phys. Status Solidi* 2 (1962) 1479.
- [6] D.A. Broido, M. Malorny, G. Birner, N. Mingo, D.A. Stewart, Intrinsic lattice thermal conductivity of semiconductors from first principles, *Appl. Phys. Lett.* 91 (2007) 231922.
- [7] L. Lindsay, C. Hua, X.L. Ruan, S. Lee, Survey of ab initio phonon thermal transport, *Mater. Today Phys.* 7 (2018) 106.
- [8] T. Feng, X. Ruan, Higher-order phonon scattering: advancing the quantum theory of phonon linewidth, thermal conductivity and thermal radiative properties, in: *Nanoscale Energy Transport*, IOP Publishing, 2020, pp. 2-1-2-44.
- [9] Y. Xia, V.I. Hegde, K. Pal, X. Hua, D. Gaines, S. Patel, J. He, M. Aykol, C. Wolverton, High-throughput study of lattice thermal conductivity in binary rocksalt and zinc blende compounds including higher-order anharmonicity, *Phys. Rev. X* 10 (2020): 041029.
- [10] Y. Xia, K. Pal, J. He, V. Ozoliņš, C. Wolverton, Particlelike phonon propagation dominates ultralow lattice thermal conductivity in crystalline Ti3VS4, *Phys. Rev. Lett.* 124 (2020): 065901.
- [11] T. Feng, X. Ruan, Prediction of spectral phonon mean free path and thermal conductivity with applications to thermoelectrics and thermal management: a review, *J. Nanomater.* 2014 (2014) 1.
- [12] T. Feng, X. Ruan, Quantum mechanical prediction of four-phonon scattering rates and reduced thermal conductivity of solids, *Phys. Rev. B* 93 (2016): 045202.
- [13] T. Feng, L. Lindsay, X. Ruan, Four-phonon scattering significantly reduces intrinsic thermal conductivity of solids, *Phys. Rev. B* 96 (2017) 161201.
- [14] L. Lindsay, D.a. Broido, T.L. Reinecke, First-principles determination of ultrahigh thermal conductivity of boron arsenide: a competitor for diamond? *Phys. Rev. Lett.* 111 (2013): 025901.
- [15] J.W.L. Pang, W.J.L. Buyers, A. Chernatynskiy, M.D. Lumsden, B.C. Larson, S.R. Phillpot, Phonon lifetime investigation of anharmonicity and thermal conductivity of UO2 by neutron scattering and theory, *Phys. Rev. Lett.* 110 (2013) 157401.
- [16] K. Gofryk, S. Du, C.R. Stanek, J.C. Lashley, X.-Y. Liu, R.K. Schulze, J.L. Smith, D.J. Safarik, D.D. Byler, K.J. McClellan, B.P. Uberuaga, B.L. Scott, D.A. Andersson, Anisotropic thermal conductivity in uranium dioxide, *Nat. Commun.* 5 (2014) 4551.
- [17] G. Kaur, P. Panigrahi, M.C. Valsakumar, Thermal properties of UO2 with a non-local exchange-correlation pressure correction: a systematic first principles DFT + U study, *Model. Simulat. Mater. Sci. Eng.* 21 (2013) 065014.
- [18] Y. Yun, D. Legut, P.M. Oppeneer, Phonon spectrum, thermal expansion and heat capacity of UO2 from first-principles, *J. Nucl. Mater.* 426 (2012) 109.
- [19] B.-T. Wang, P. Zhang, R. Lizárraga, I. di Marco, O. Eriksson, Phonon spectrum, thermodynamic properties, and pressure-temperature phase diagram of uranium dioxide, *Phys. Rev. B* 88 (2013) 104107.
- [20] H. Kim, M. Kim, M. Kaviani, Lattice thermal conductivity of UO2 using ab-initio and classical molecular dynamics, *J. Appl. Phys.* 115 (2014) 123510.
- [21] S.-Y. Yue, X. Zhang, G. Qin, S.R. Phillpot, M. Hu, Metric for strong intrinsic fourth-order phonon anharmonicity, *Phys. Rev. B* 95 (2017) 195203.
- [22] E. Torres, I. Cheikhjifon, T.P. Kaloni, J. Pencer, A comparative Analysis of the phonon properties in UO2 using the Boltzmann transport equation coupled with DFT + U and empirical potentials, *Comput. Mater. Sci.* 177 (2020) 109594.
- [23] X. Zhu, R. Gao, H. Gong, T. Liu, D.Y. Lin, H. Song, UO2/BeO interfacial thermal resistance and its effect on fuel thermal conductivity, *Ann. Nucl. Energy* 154 (2021) 108102.
- [24] Y. Xia, V. Ozoliņš, C. Wolverton, Microscopic mechanisms of glasslike lattice thermal transport in cubic Cu12Sb4 S13 tetrahedrites, *Phys. Rev. Lett.* 125 (2020) 43.
- [25] L. Lindsay, D.a. Broido, N. Mingo, Flexural phonons and thermal transport in graphene, *Phys. Rev. B* 82 (2010) 115427.
- [26] T. Feng, X. Ruan, Four-phonon scattering reduces intrinsic thermal conductivity of graphene and the contributions from flexural phonons, *Phys. Rev. B* 97 (2018): 045202.
- [27] M. Simoncelli, N. Marzari, F. Mauri, Unified theory of thermal transport in crystals and glasses, *Nat. Phys.* 15 (2019) 809.
- [28] M. Simoncelli, N. Marzari, F. Mauri, Wigner formulation of thermal transport in solids, *Arxiv* 2112 (2021): 06897.
- [29] Y. Xia, Revisiting lattice thermal transport in PbTe: the crucial role of quartic anharmonicity, *Appl. Phys. Lett.* 113 (2018): 073901.
- [30] N.K. Ravichandran, D. Broido, Unified first-principles theory of thermal properties of insulators, *Phys. Rev. B* 98 (2018): 085205.
- [31] J.K. Fink, Thermophysical properties of uranium dioxide, *J. Nucl. Mater.* 279 (2000) 1.
- [32] J.L. Bates, Visible and infrared absorption spectra of uranium dioxide, *Nucl. Sci. Eng.* 21 (1965) 26.
- [33] T.G. Godfrey, W. Fulkerson, T.G. Kollie, J.P. Moore, D.L. McELROY, Thermal conductivity of uranium dioxide from -57° to 1100°C by a radial heat flow technique, *J. Am. Ceram. Soc.* 48 (1965) 297.
- [34] C. Ronchi, M. Sheindlin, D. Staicu, M. Kinoshita, Effect of burn-up on the thermal conductivity of uranium dioxide up to 100.000 MWd-t, *J. Nucl. Mater.* 327 (2004) 58.
- [35] Z. Liu, X. Yang, B. Zhang, W. Li, High thermal conductivity of wurtzite boron arsenide predicted by including four-phonon scattering with machine learning potential, *ACS Appl. Mater. Interfaces* 13 (2021) 53409.
- [36] A. McGaughey, M. Kaviani, Quantitative validation of the Boltzmann transport equation phonon thermal conductivity model under the single-mode relaxation time approximation, *Phys. Rev. B* 69 (2004): 094303.
- [37] A.J.H. McGaughey, M. Kaviani, Phonon transport in molecular dynamics simulations: formulation and thermal conductivity prediction, *Adv. Heat Tran.* 39 (2006) 169.
- [38] S. Yamasaki, T. Arima, K. Idemitsu, Y. Inagaki, Evaluation of thermal conductivity of hyperstoichiometric UO2+x by molecular dynamics simulation, *Int. J. Thermophys.* 28 (2007) 661.
- [39] S. Nichenko, D. Staicu, Thermal conductivity of porous UO2: molecular dynamics study, *J. Nucl. Mater.* 454 (2014) 315.
- [40] S. Du, K. Gofryk, D.A. Andersson, X.-Y. Liu, C.R. Stanek, A Molecular Dynamics Study of Anisotropy and the Effect of Xe on UO2 Thermal Conductivity, Los Alamos National Lab.(LANL), 2013.
- [41] P.S. Ghosh, P.S. Somayajulu, K. Krishnan, N. Pathak, A. Arya, G.K. Dey, Thermal expansion and thermal conductivity of (Th,U)O2 mixed oxides: a molecular dynamics and experimental study, *J. Alloys Compd.* 650 (2015) 165.
- [42] E. Jin, C. Liu, H. He, The influence of microstructures on the thermal conductivity of polycrystalline UO2, in: *International Conference on Nuclear Engineering, Proceedings, ICONE 1*, 2016, p. 1.
- [43] M.R. Tonks, X.Y. Liu, D. Andersson, D. Perez, A. Chernatynskiy, G. Pastore, C.R. Stanek, R. Williamson, Development of a multiscale thermal conductivity model for fission gas in UO2, *J. Nucl. Mater.* 469 (2016) 89.
- [44] W. Chen, M.W.D. Cooper, Z. Xiao, D.A. Andersson, X.M. Bai, Effect of Xe bubble size and pressure on the thermal conductivity of UO2 - a molecular dynamics study, *J. Mater. Res.* 34 (2019) 2295.
- [45] X. Zhu, H. Gong, Y.F. Zhao, D.Y. Lin, G. Han, T. Liu, H. Song, Effect of Xe bubbles on the thermal conductivity of UO2: mechanisms and model establishment, *J. Nucl. Mater.* 533 (2020) 152080.
- [46] W. Chen, X.M. Bai, Unified effect of dispersed Xe on the thermal conductivity of UO2 predicted by three interatomic potentials, *JOM (J. Occup. Med.)* 72 (2020) 1710.
- [47] C.A. Dennett, W.R. Deskins, M. Khafizov, Z. Hua, A. Khanolkar, K. Bawane, L. Fu, J.M. Mann, C.A. Marianetti, L. He, D.H. Hurley, A. El-Azab, An integrated experimental and computational investigation of defect and microstructural effects on thermal transport in thorium dioxide, *Acta Mater.* 213 (2021) 116934.
- [48] C.A. Dennett, Z. Hua, A. Khanolkar, T. Yao, P.K. Morgan, T.A. Prusnick, N. Poudel, A. French, K. Gofryk, L. He, L. Shao, M. Khafizov, D.B. Turner, J.M. Mann, D.H. Hurley, The influence of lattice defects, recombination, and clustering on thermal transport in single crystal thorium dioxide, *Apl. Mater.* 8 (2020).
- [49] R.A. Wolfe, S.F. Kaufman, *MECHANICAL PROPERTIES OF OXIDE FUELS, LSBR/LWB DEVELOPMENT PROGRAM*, 1967.
- [50] T. Feng, X. Yang, X. Ruan, Phonon anharmonic frequency shift induced by four-phonon scattering calculated from first principles, *J. Appl. Phys.* 124 (2018) 145101.
- [51] S. Motoyama, Y. Ichikawa, Y. Hiwatari, A. Oe, Thermal conductivity of uranium dioxide by nonequilibrium molecular dynamics simulation, *Phys. Rev. B* 60 (1999) 292.
- [52] T. Watanabe, S.B. Sinnott, J.S. Tulenko, R.W. Grimes, P.K. Schelling, S.R. Phillpot, Thermal transport properties of uranium dioxide by molecular dynamics simulations, *J. Nucl. Mater.* 375 (2008) 388.
- [53] T. Uchida, T. Sunaoshi, M. Kato, K. Konashi, Thermal properties of UO2 by molecular dynamics simulation, *Prog. Nucl. Sci. Technol.* 2 (2011) 598.
- [54] B. Deng, A. Chernatynskiy, P. Shukla, S.B. Sinnott, S.R. Phillpot, Effects of edge dislocations on thermal transport in UO2, *J. Nucl. Mater.* 434 (2013) 203.
- [55] M.J. Qin, M.W.D. Cooper, E.Y. Kuo, M.J.D. Rushton, R.W. Grimes, G.R. Lumpkin, S.C. Middleburgh, Thermal conductivity and energetic recoils in UO2 using a many-body potential model, *J. Phys. Condens. Matter* 26 (2014) 495401.
- [56] X.Y. Liu, M.W.D. Cooper, K.J. McClellan, J.C. Lashley, D.D. Byler, B.D.C. Bell, R.W. Grimes, C.R. Stanek, D.A. Andersson, Molecular dynamics simulation of thermal transport in UO2 containing uranium, oxygen, and fission-product defects, *Phys. Rev. Appl.* 6 (2016) 044015.

- [57] M.W.D. Cooper, C.R. Stanek, X.Y. Liu, D.A. Andersson, A comment on the thermal conductivity of (U,Pu)O₂ and (U,Th)O₂ by molecular dynamics with adjustment for phonon-spin scattering, *MRS Adv.* 1 (2016) 2483.
- [58] M. Jin, M. Khafizov, C. Jiang, S. Zhou, C.A. Marianetti, M.S. Bryan, M.E. Manley, D.H. Hurley, Assessment of empirical interatomic potential to predict thermal conductivity in ThO₂ and UO₂, *J. Phys. Condens. Matter* 33 (2021) 275402.
- [59] E. Eser, H. Koc, M. Gokbulut, G. GURSOY, Estimations of heat capacities for actinide dioxide: UO₂, NpO₂, ThO₂, and PuO₂, *Nucl. Eng. Technol.* 46 (2014) 863.
- [60] A. Jain, A.J.H. McGaughey, Effect of exchange–correlation on first-principles-driven lattice thermal conductivity predictions of crystalline silicon, *Comput. Mater. Sci.* 110 (2015) 115.
- [61] D. Vanderbilt, S.S.G. Louie, M.L.M. Cohen, Calculation of anharmonic phonon couplings in C, Si, and Ge, *Phys. Rev. B* 33 (1986) 8740.
- [62] T. Feng, L. Lindsay, X. Ruan, Four-phonon scattering significantly reduces intrinsic thermal conductivity of solids, *Phys. Rev. B* 96 (2017) 161201.
- [63] Y. Luo, X. Yang, T. Feng, J. Wang, X. Ruan, Vibrational hierarchy leads to dual-phonon transport in low thermal conductivity crystals, *Nat. Commun.* 11 (2020) 2554.